GeoJournal of Tourism and Geosites
ISSN 2065-1198, E-ISSN 2065-0817

Year XVI, vol. 46, no. 1, 2023, p.304-314
DOI 10.30892/gtg.46134-1028

ENVIRONMENTAL IMPACTS OF URBAN SPRAWL USING REMOTE SENSING INDICES: A CASE STUDY OF AMMAN CITY – THE CAPITAL OF JORDAN

Nour ABDELJAWAD*
Hungarian University of Agriculture and Life Sciences, Doctoral School of Management and Organizational Sciences, Kaposvár, Hungary, e-mail: Nour.Abdeljawad@phd.uni-mate.hu

Victor ADEDOKUN
Department of Urban and Regional Planning, Modibbo Adama University, Yola, Nigeria, e-mail: mayowaadedokunvictor@gmail.com

Imre NAGY
University of Novi Sad, Department of Geography, Tourism and Hotel Management, Faculty of Science, Novi Sad, Serbia, e-mail: imre.nadj@dgt.uns.ac.rs

Citation: Abdeljawad, N., Adedokun, V., & Nagy, I. (2023). ENVIRONMENTAL IMPACTS OF URBAN SPRAWL USING REMOTE SENSING INDICES: A CASE STUDY OF AMMAN CITY – THE CAPITAL OF JORDAN. *GeoJournal of Tourism and Geosites*, 46(1), 304–314. https://doi.org/10.30892/gtg.46134-1028

Abstract: Urban sprawl is known to have a negative impact on the environment and is considered one of the main challenges in urban development. The current work aims to understand the spatio-temporal characteristics of urban growth and its environmental impact in the city of Amman. The paper's empirical method relies on NDVI, NDBI, and LST calculated using remote sensing and GIS techniques. For this study, Landsat Thematic Mapper Landsat 5-TM images from 1990, 1995, 1999, and 2004 were acquired, as well as Landsat 8-OLI images from 2013, 2017, and 2022. The surface temperature of Amman has increased as the area of paved roads, residential, commercial and industrial land use types have increased, while green spaces and vacant lots have decreased. The NDVI analysis revealed that there was variation in the vegetation index during the study year due to human activities as well as climatic change. Correlations between biophysical variables and LST revealed that NDVI had a significant negative correlation, while NDBI had a positive relationship. Further, a significant positive correlation was observed between road networks and built-up areas which enhance the occurrence of urban sprawl due to urbanization. This study highlighted the significance of considering the environmental consequences of urban sprawl when developing and implementing GAM policies and strategies.

Key words: Urban sprawl, Remote Sensing (RS), land surface temperature (LST), Normalized Difference Vegetation index (NDVI), Normalized Difference Building index (NDBI), Pearson correlation, Greater Amman Municipality (GAM)

* * * * * *

INTRODUCTION

According to a United Nations report, more than 55% of the world's population currently resides in urban areas and by 2050 this percentage is expected to rise to 67% (United Nations, 2018). Urbanization has a detrimental effect on the environment and is a sign of socio-economic and political growth. Loss of vegetation, which results in the release of greenhouse gases like CO_2 into the environment, is one effect of urban expansion and sprawl on the environment (Correia Filho et al., 2021; Dobbs et al., 2017). According to (Al-Kofahi et al., 2018a), between 2003 and 2015, urban expansion reduced agricultural land in the city of Amman by 50 per cent (agriculture land represent around 14% of Greater Amman area). The increase in the planet's average surface temperature over the past century has been well-documented as a factor in global warming. This warming is a result of the conversion of green space into urban areas, rising carbon dioxide levels, and increased emissions of other pollutants, all of which are generally attributed to increased human activity (Kaplan et al., 2018). For this reason, it's important to comprehend and research how urban sprawl affects the ecosystem and the environment. Amman city continued to grow, reaching a population of 2.5 million over 680 km^2 by the middle of the 2000s, and today it is a metropolis of 800 km^2. Amman's urban area increased by 61.73%, from 147.08km^2 in 1987 to 237.86km^2 in 2017. Another notable change is the ongoing reduction in the vegetation area within GAM, which occupied 35.22 km^2 in 1987 and decreased to 16.40 km^2 in 2017, representing a decrease of 18.82 km^2 or 53.54% (Al-Bilbisi, 2019). Amman's rapid population growth is caused by a variety of factors, including rural-urban migration, the capital's concentration of economic activities and services, and, most importantly refugee influx.

Urbanization and rapid growth of the population, have resulted in the alteration of other land uses, particularly vegetated surfaces, to impervious surfaces, are already having an impact on the environment in a variety of ways, including the increase in LST, which can be considered one of the major causes of unplanned and unsustainable and change in land cover in cities (Semeraro et al., 2021; Gazi et al., 2021; Nse et al., 2020; Al-Kofahi et al., 2018a; Al-Kofahi et al., 2018b; Jaber,2018; Patarkalashvili, 2017). As a result, scientists and urban planners are very interested in vegetation, because

* Corresponding author

vegetation plays many important roles in urban systems (Semeraro et al., 2021). Numerous environmental advantages of vegetation include lowering the ambient temperature, lowering air pollution (Janhäll, 2015), decreasing the urban heat island effect (Aboelata and Sodoudi, 2020), decreasing the risk of flooding (Richards and Belcher, 2020; Yan et al., 2016), and reducing noise pollution (Han et al., 2018). Urban vegetation has emerged as one of the most significant potential solutions to a number of urban challenges to support the goal of sustainable development in cities (Cox et al., 2018). In light of this, studying urban vegetation has benefits for both the environment and socio-economic development.

Urban environmental indicators can be calculated using conventional data, but these data are frequently insufficient because of generalization, outdated, or lack of availability. In contrast, Earth observation has established itself as a viable alternate resource of geo-information for environmental monitoring and urban development, adding to scientific understanding by supplying the spatial data required to carry out urban planning projects. The actual advantage of satellite technology over traditional methods is that urban geospatial information can offer effective alternative planning methods and tools by helping in the development of cost effective, precise, and time-efficient urban environmental indicators (Chrysoulakis et al., 2014). For instance, it helps in the analysis of spatiotemporal trends of Earth's surface temperature and can also help assess the impact of road network on urban sprawl and the environment which aids in the assessment of environmental changes (Zhan and Ukkusuri, 2019). Remote sensing (RS) techniques can be employed to acquire "vegetation indices" and then use them to assess vegetation cover. Meanwhile, the NDVI is a popular tool for extracting vegetation. The higher the values of the NDVI imply a greater amount of vegetation in a pixel. Furthermore, the NDBI has been commonly employed in the extraction of urban areas. Researching the relationship between LST and the land cover could be useful for understanding urban environment (Kaplan et al., 2018). The relationship between temperature and NDVI in vegetation is well-established. Whereas the NDVI is deemed as crucial indicator for urban environment (Abebe et al., 2021). Nevertheless, Studies revealed a negative relationship between NDVI and LST (Abdullah et al., 2022; Gui et al., 2019; Deng et al., 2018). In respect to built-up areas, urban density and Ground imperviousness is another aspect that raises temperatures (Momin et al., 2022). NDBI and LST are found to be positively correlated (Kaplan et al., 2018).

Urban areas require the monitoring of land surface temperatures because high temperatures result in higher energy costs for cooling buildings, especially during the summer (Vani and Prasad, 2020; Estoque et al., 2017). The temperature measured in the air close to the earth's surface (1m) in an open area is referred to as land surface temperature (LST). Air temperature, on the other hand, refers to the temperature measured within the atmosphere more than one kilometer above the earth's surface. LST is always greater than the air temperature. The term "land surface temperature" refers to how hot the Earth's "surface" feels to the touch in a particular location (Jaber, 2020).

Whatever a satellite observes when peering down at the earth through the atmosphere is referred to as the "surface". It might be a building's roof, grass on a lawn, snow, or perhaps leaves in a forest canopy. As a result, the temperature of the air as recorded in the daily weather report is different from the temperature of the ground surface. In general, there are two primary methods for assessing the LST phenomenon: either by (i) automatic temperature measurements derived from traditional weather stations (Kaplan et al., 2018); or (ii) temperature measurements from land surfaces which are derived from Thermal InfraRed (TIR) remote sensing data (Mushore et al., 2017; Jiménez-Muoz et al., 2014).

Studies have shown that using both built-up and vegetation indexes together can provide a clearer knowledge of the temperature of the land surface as both affect surface temperature (Momin et al., 2022; Hammed et al., 2019). Over the last three decades, Amman has experienced a significant rise in urbanization, with a rapid increase in the area land built. This trend in the increase of built-up land can determined by a variety of factors, including government policy, land use patterns, population growth, economic development, and increased road networks. An increase in population density leads to an increase in the use of transportation facilities. The sprawling city is dominated by relatively inefficient private car use, expensive public transportation systems, and high transportation-related energy consumption, all of which contribute to an increase in CO_2 emissions to the atmosphere.

Study contribution and objectives

Only a few researchers have investigated Amman's urban growth and related LULC changes, such as (Al-Bilbisi, 2019; Jaber, 2018; Al-Kofahi et al., 2018), but no research has been conducted on how these changes affect the city's surface temperature and its environmental impacts. This study adds and extends previous work such as which conducted in Amman by Jaber, 2018. The current paper attempts to fill this research gap by building on previous research and aiming to increase and nourish general understanding and knowledge about the relationship between urban sprawl and LST by establishing NDVI and NDBI as independent variables (Abdullah et al., 2022; Vani and Prasad, 2020; Gui et al., 2019; Deng et al. 2018). We filled the gap in the research by explaining the effect of LULC change on LST and vegetation in Amman. We hypothesized that more vegetation would have a lower LST value whereas, the higher NDBI would have a higher LST value. To further test the theory, we expanded our research by examining the relationships between two biophysical variables, NDVI, NDBI, and LST. Therefore, our study aims to (i) analyse the impact of urban sprawl on the environment particularly on surface temperature and vegetation, and to (ii) compare the effects of urban growth and its effects on NDVI and LST in Amman.

METHODOLOGY

1. Study area

Jordan's capital and largest city, Amman, is the nation's most populous city and the country's political, economic, and cultural hub, as illustrated in Figure 1. The research area is characterized by dense human activity, with a population of 4,061,150 as of 2021. The area is located in north-central Jordan and spans 31 25"N -32 1"N latitude and 35 66"E - 36 42"E

longitude. Amman covers an area of 800 km2 and has elevations ranging from 700 to 1,100 meters above mean sea level (Al-Kofahi et al., 2018a; Abdeljawad et al., 2022). Amman's topography is characterized by narrow valleys and steep hills. Amman falls under the semi-arid climate category because of its proximity to the Mediterranean climate zone. Summers are mildly long, warm, and breezy. Winter typically begins around the end of November and lasts until early to mid-March. Snow may fall in Amman's western and northern districts (≥ 1,000 m above sea level). The majority of the rain falls between November and April, with an annual rainfall average of 300 mm. Amman has grown significantly in terms of geopolitical status, physical land, and population over the last century (Potter et al., 2009). Urban areas in Amman expanded at the expense of other land use land cover classes, particularly vegetation lands, as a result of urban growth that occurred along transportation networks away from the city center (Al-Bilbisi, 2019). Unexpected urban growth has resulted in a number of environmental and infrastructure problems, necessitating the urgent need for monitoring and managing the city using spatial techniques.

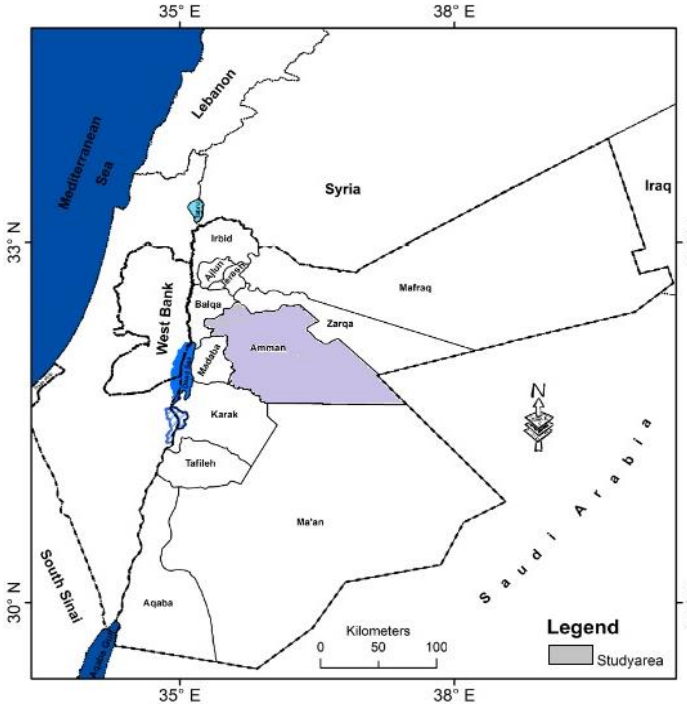

Figure 1. The geographic location of Amman (Source: Khawaldah, 2016)

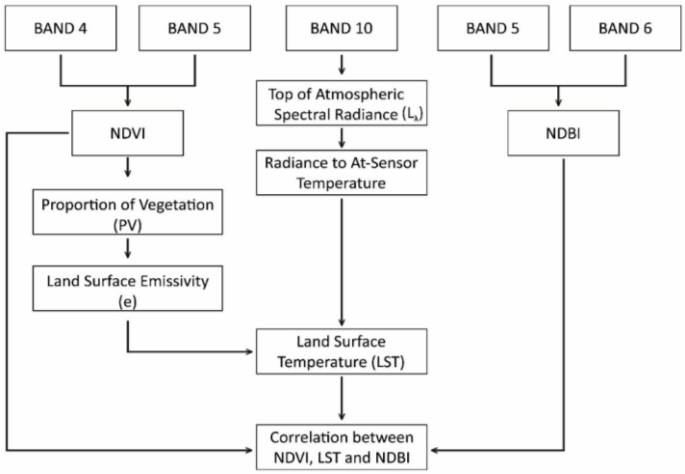

Figure 3. Methodological Flowchart for Landsat 8-OLI satellite imagery

2. MATERIALS AND METHODS

The current study's overall methodology is illustrated in a flowchart (Figure 2 for Landsat 5-TM satellite imagery and Figure 3 for Landsat 8-OLI satellite imagery).

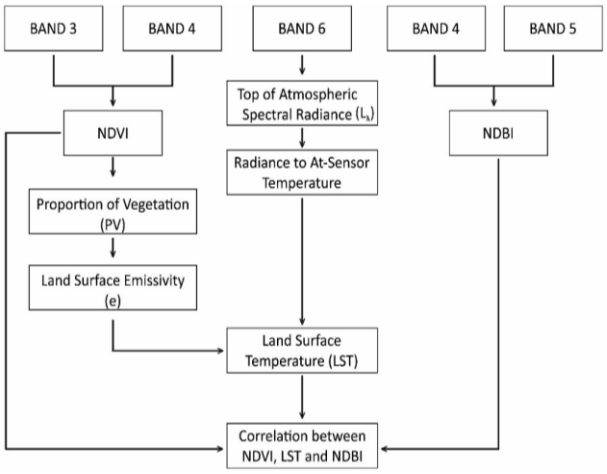

Figure 2. Methodological Flowchart for Landsat 5-TM satellite imagery

The analysis of Land surface temperature involves the application of TIR, RS, NIR data, as well as the red band, were also used to generate the NDVI which serves as an input for analyzing the land surface temperature. Both MIR and NIR were utilized to extract the built-up index. A series of Landsat images having a 3-dimensionial resolution (30×30 m) were acquired from the United States Geological Survey (USGS).

The road network of Amman city for the study year (1990 - 2022) were digitized from existing aerial photographs. On the other hand, data on the spatial extent of urbanized area in Amman city was extracted from the LULC archives (as shown on supplementary document). The Landsat 5-TM and Landsat 8-OLI were attained in the current study for the years 1990, 1995, 1999, and 2004 and 2013, 2017, and 2022, respectively, since they offer a suitable and economical source of data for a variation of applications, comprising study of the vegetation index, land surface temperature, and built-up index.

The spatial scope of the study region was then subset into the imagery (data sets). Table 1 demonstrates the specifications of the satellite image bands, wavelength, resolution, and acquisition date. Time series air temperature data were obtained from the National Aeronautics and Space Administration (NASA) and also from the Jordan meteorological department as shown in table 2. The outcomes of this data analysis were contrasted with those of the analysis of land surface temperature.

3. Derivation of Normalized Difference Vegetation Index (NDVI)

In 1973, the NDVI that was introduced by Rouse et al., (1973), has been frequently utilized to collect as well as investigating the dynamics of urban vegetation and to monitor urban growth (Jaber, 2018; El Garouani et al., 2017; Escobedo et al., 2016). The NDVI measures the amount of vegetation by comparing the NIR (which vegetation

significantly reflects) and red-light contrasts (which vegetation absorbs) (Kundu et al., 2021). The NDVI for the investigated area was calculated using the map algebra function (raster calculator) of ArcGIS Pro 2.5. It is represented mathematically using the formula (Rouse et al.,1974) as shown below:

$$NDVI = \frac{NIR - RED}{NIR + RED}$$

Where, NIR corresponds to band 4 for Landsat-5 TM and band 5 for Landsat-8 OLI photos, whereas red corresponds to band 3 for Landsat-5 TM and band 4 for Landsat-8 OLI images.

The NDVI readings are always between -1 and +1. However, each form of land cover does not have a clear limit. If the NDVI value is near to +1, there is a good chance that the plant's densely packed leaves are green (dense vegetation), values between 0.4 and 0.7 depict typical, healthy vegetation, and values between 0.18 to 0.27 corresponds to shrubs or grassland. Whereas negative values represent water bodies and highly dense urban areas. Values close to 0 show that there are no green covers rather it is likely to be an urbanized area. In general, readings between -0.1 and 0.18 are indicative of desert, a rock outcrop, sand, or snow (Ullah et al., 2020).

$$NDVI\ (Landsat - 5\ TM) = \frac{B4-B3}{B4+B3}$$

$$NDVI\ (Landsat - 8\ OLI\ ) = \frac{B5 - B4}{B5 + B4}$$

Table 1. Satellite image specification of Landsat 5-TM and Landsat 8-OLI (i.e., image bands, wavelength, resolution, and acquisition date) (Source: Adapted from http://glovis.usgs.gov. 18th July 2022)

Image Specification		
Image Type	Landsat 5-TM	Landsat 8-OLI
Swath width (Km)	185	185
Spectral range (μm)	Red (3) Band (0.63-0.69) NIR (4) Band (0.76-0.90) MIR (5) Band (1.55-1.75) TIR (6) Band (10.4 0-12.50)	Red (4) Band (0.630-0.680) NIR (5) Band (0.845-0.885) MIR (6) Band (1.57-1.65) TIR (10) Band (10.60-11.19)
Resolution (m)	30	30
Acquisition date	1990-07-21 1995-07-19 1999-07-14 2004-07-11	2013-07-04 2017-07-15 2022-07-13
Revisit time (day)	16	16
Cloud cover (%)	0.00	0.00

Table 2. Air temperature data (Source: National Aeronautics and Space Administration,NASA, Jordan meteorological department)

Month	YEAR	Mini. Temp (ºC)	Max. Temp. (ºC)
July	1990	19.25	40.87
July	1995	20.51	41.37
July	1999	19.58	40.45
July	2004	19.99	43.88
July	2013	19.87	40.02
July	2017	21.23	45.05
July	2022	19	39

4. Derivation of Normalized Difference Built-up Index (NDBI)

For the NDBI, it can computes the built-up area by measuring the difference among middle-infrared and NIR. The NIR and MIR bands are used by NDBI to emphasise man-made built-up areas. It is ratio-based to decrease the effects of changes in the illumination of the ground and atmospheric influences. The reflectance increases dramatically from the NIR to the MIR band in the built-up areas and arid country. However, vegetation has a somewhat bigger or smaller DN value (insignificant) on MIR compared to NIR. And this can be observed as the distinct increase between these bands. As a result, after differencing and binary recoding, the build-up region may be distinguished from the other covers and hence from the NDBI Pixel values of typical land covers (Xu et al., 2017). Positive values for build-up pixels are obtained via standardized MIR and NIR differentiation. For the current investigated area, the NDBI was calculated using the map algebra function (raster calculator) of ArcGIS Pro 2.5. It is represented mathematically using the formula below:

$$NDBI = \frac{MIR - NIR}{MIR + NIR}$$

whereas NIR is band 4 for Landsat-5 TM and band 5 for photos from Landsat-8 OLI, MIR is band 5 for Landsat-5 TM and band 6 for images from Landsat-8 OLI.

$$NDBI\ (Landsat - 5\ TM) = \frac{B5 - B4}{B5 + B4} \qquad NDBI\ (Landsat - 8\ OLI\ ) = \frac{B6 - B5}{B6 + B5}$$

5. Land Surface Temperature (LST)

The application of LST is employed to analyze any impact of LULC and urbanization changes on temperature. Estimating the LST comprises various procedures and steps that are been described by NASA (USGS, 2019b). These procedures range from the transformation of DN to At-sensor spectral radiance, conversion of radiance to At-satellite brightness temperature, to the normalized difference vegetation index, proportional vegetation, and land surface emissivity among others which are described below:

5.1. The conversion of digital number (DN) to At-sensor spectral radiance

The DN of thermal infrared band is converted into L_λ using the equation taken from the USGS webpage. The calibration parameters can be retrieved from metadata of the satellite image (USGS, 2019a).

$$L_\lambda = M_L\ x\ Q_{cal} + A_L \quad (1)$$

where L denotes TOA Spectral Radiance, M_L denotes Radiance M_{ult}-band x, A_L denotes Radiance Add band x, and Q_{cal} is the quantized and calibrated standard product pixel (thermal band).

5.2. The conversion of radiance (L_λ) to At-satellite brightness temperature (T_{sat})

This involves the conversion of L_λ to T_{sat} so as to obtain the actual temperature received by the satellite during the time when the image is captured. Equation (2) can be used to convert the thermal band data from at-sensor spectral radiance to effective At-sensor brightness temperature (USGS, 2019b).

$$T_{sat} = \left[\frac{K_2}{ln\, ln\,(\frac{K_1}{L_\lambda}+1)}\right] - 272.15 \quad (2)$$

where T_{sat} is the At-satellite brightness temperature, L_λ is the TOA Spectral radiance, K_1 represents the K_1 constant of band x, and K_2 presents the K_2 constant of band x. **Note:** The K_1 and K_2 factors can be recovered from the image meta data.

5.3. Derivation of Land Surface Emissivity (LSE)

LSE is a crucial surface parameter that may be calculated from radiance emitted from space measurements since it is a characteristic of natural materials. The TIR data from satellites is the primary resource for assessing a region's surface emissivity. It could be employed to estimate surface emissivity using satellite data with high spatial resolution, such as TIR bands from Landsat images (Chakraborty, 2021). The land surface emissivity is an essential factor for estimating the land surface energy budget and determining the land surface temperature from remote sensing data (Nse et al., 2020). The land surface emissivity is computed using Eq. 3 below (Abdullah et al., 2022; Imran et al., 2021; Ullah et al., 2020; Kumari et al., 2018)

$$e = 0.004PV + 0.986 \quad (3)$$

where, e is the Land surface emissivity, PV presents the Proportional Vegetation, Note, and PV is computed from NDVI using Eq. 4 below:

$$PV = \left(\frac{NDVI - NDVI_{min}}{NDVI_{max} - NDVI_{min}}\right)^2 \quad (4)$$

where, PV describes the Proportional Vegetation, NDVI shows the Normal difference vegetation index, $NDVI_{min}$ presents the Minimum NDVI value, and $NDVI_{max}$ is the Maximum NDVI value.

The final Land Surface Temperature (LST) is estimated using the single Mono-window (Ullah et al., 2020; Kumari et al, 2018) as stated in Eq. 5 below:

$$LST = \frac{T_{sat}}{1+\left(\lambda+\frac{T_{sat}}{p}\right) X \ln \ln e} \quad (5)$$

where, LST is the Land surface temperature, T_{sat} is the At-satellite brightness temperature, λpresents the Wave length of emitted radiance (thermal band), P is a constant (14380), and e represents the Land surface emissivity.

RESULT AND DISCUSSION

1. NDVI analysis using Landsat imagery

The usefulness of the NDVI index in monitoring vegetation cover and satellite analysis has been sufficiently established during the past two decades. The NDVI values of the pixels range from -1 to +1. A wider variety of healthy plants is indicated by higher NDVI readings. NDVI's analysis shows that in 1990 the study area has a minimum value of -0.52 and a maximum value of 0.72. In 1995 there was a minimum value of NDVI of -0.24 and a maximum value of 0.58. In the meantime, in 1999, the study area has a minimum value of -0.21 and a maximum value of 0.61, while in 2004 there was a minimum NDVI value of -0.60 and a maximum value of 0.82 was. In addition, Amman City has a minimum value of -0.19 and a maximum value of 0.42 in 2013, while in 2017 a minimum value of -0.16 and a maximum value of 0.47, finally, in the year 2022, there was a minimum value of -0.24 and a maximum value of 0.59. In 2013, less value of NDVI may have been as a result of distortion in the ecosystem due to urbanization.

2. Analysis of NDBI using Landsat Imagery

The built-up index within Amman City was extracted using the relationship between the MIR and NIR bands of Landsat 5-TM and Landsat 8-OLI for the study year period (1990-2022). The findings demonstrate that in 1990, the investigated area had a minimum NDBI value of −1.0 and a maximum value of 0.51, in the year 1995 there was a minimum NDBI value of −0.81 and a maximum value of 0.56, in 1999 there was a minimum NDBI value of -0.99 and a maximum value of 0.76, in 2004 there was a minimum NDBI value of -1.0 and a maximum value of 0.81, In 2013 there was a minimum NDBI value of -0.69 and a maximum value of 0.53, in 2017 there was a minimum NDBI value of -0.79 and a maximum value of 0.25, most recently in 2022 a minimum NDBI value of -0.94 and a maximum value of 0.42.

3. Estimation of LST using Thermal band of Landsat Imagery

As previously explained, the LST was computed at the landscape level for both the Landsat TM and OLI thermal bands. Figure 4 depicts the minimum and maximum temperatures derived from Landsat TM and OLI data. Figure 4 depicts a consistent increase in the maximum temperature of the land surface within the investigated area from 39.50^{0}C in 1990 to 46.00 in 2022, with the highest temperature recorded in 2017 (51.60^{0}C). The conversion of vegetation, agricultural land, and bare surface into urban centers to accommodate the expanding population is the likely cause of this steady rise in land temperature over the course of the study year. Figure 5-11 depicts the spatial distribution of LST across Amman during the research period.

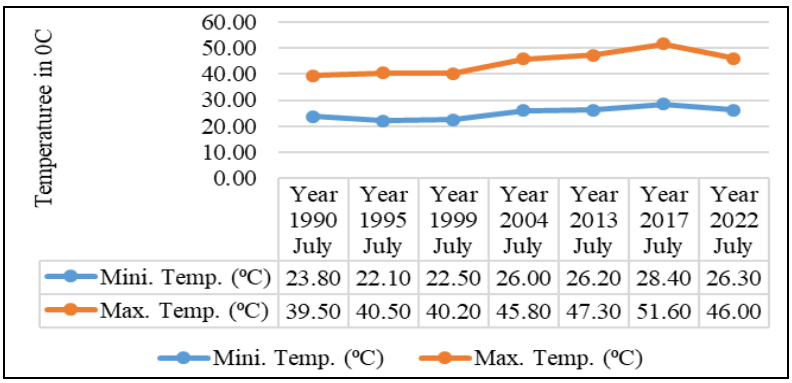

Figure 4. Result of LST analysis of Amman city from 1990 – 2022 (Source: Authors primary data Analysis, 2022. Data Source: Thermal band of Landsat Imageries used)

From Figure 5, Image A, B, C represent the NDVI, NDBI and LST of the investigated area in 1990 respectively. From the result of the LST (image C), built-up area (in city center) recorded the highest land temperature in July 1990, which is shown graphically in figure 5 above, with a temperature range of 33.9^{0}C - 39.5^{0}C. Because of the presence of agricultural land and bare surface, the northern, southern, and eastern parts of the study area recorded the lowest land temperature in 1990, with a temperature range of 23.8^{0}C - 29.5^{0}C.

As shown graphically in figure 6, image A, B, C represent the NDVI, NDBI and LST of the study area in 1995 respectively. From the result of the LST (image C), the built-up area (city center) recorded the highest land temperature in

July 1995 with a temperature range between 32.2ºC – 40.5ºC. The eastern, northern, and southern regions of the investigated area recorded the least land temperature in the year 1995 with a temperature range between 22.1ºC – 33.1ºC.

From Figure 7, image A, B, C represent the NDVI, NDBI and LST of the investigated area in 1999 respectively. From the result of the LST (image C), the built-up area (city center) recorded the highest land temperature in 1999 with a temperature range between 33.2ºC – 40.2ºC. The eastern, northern, and southern parts of the investigated area recorded the least land temperature in year 1999 with a temperature range between 22.5ºC – 29.6ºC. As seen graphically in figure 8 above, image A, B, C represent the NDVI, NDBI and LST of the investigated area in 2004 respectively.

From the result of the LST (image C), the built-up area (city center) recorded the highest land temperature in July 2004 with a temperature range between 38.0ºC – 45.8ºC. The eastern, northern, and southern parts of the investigated area recorded the least land temperature in the year 2004 with a temperature range between 26.0ºC – 33.9ºC. As illustrated graphically in figure 9, image A, B, C represent the NDVI, NDBI and LST of the investigated area in 2013 respectively.

From the result of the LST (image C), the built-up area in the city center, recorded the highest land temperature in July 2013, with a temperature range of 38.9^{0}C - 47.3^{0}C. Because of the presence of vegetated and bare land, the eastern, northern, and southern parts of the investigated area recorded the lowest land temperature in 2013, with a temperature ranging from 26.2^{0}C to 34.6^{0}C.

Figure 10 (image C) depicts the built-up area in city center recorded the highest land temperature in July 2017 with a temperature range between 42.4^{0}C and 51.6^{0}C due to the absence of vegetated land. whereas the southern, northern, and eastern parts of the investigated area recorded the lowest land temperature in the year 2017 with a temperature range between 28.4^{0}C and 37.7^{0}C.

From figure 11, image A, B, C represent the NDVI, NDBI and LST of the investigated area in 2022 respectively. From the result of the LST (image C), the built-up area (city center) recorded the highest land temperature in July 2022 with a temperature range between 38.2ºC – 46.0ºC, part of the north-east, south-west and north-western region of Amman recorded the lowest land temperature in the year 2022 with a temperature range between 26.3ºC – 34.1ºC as a result of the existence of vegetated and bare land.

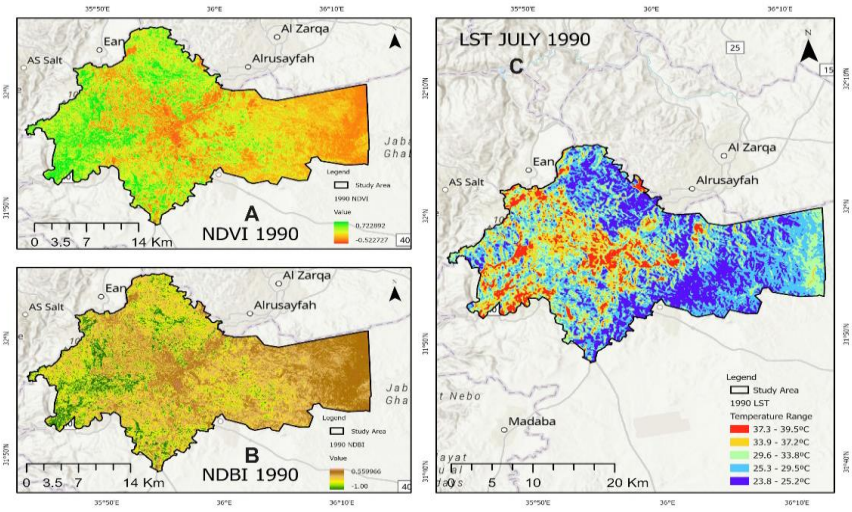

Figure 5. Amman's spatial distribution of NDVI (A), NDBI (B), and LST (C) in 1990 (Source: Authors primary data Analysis, 2022)

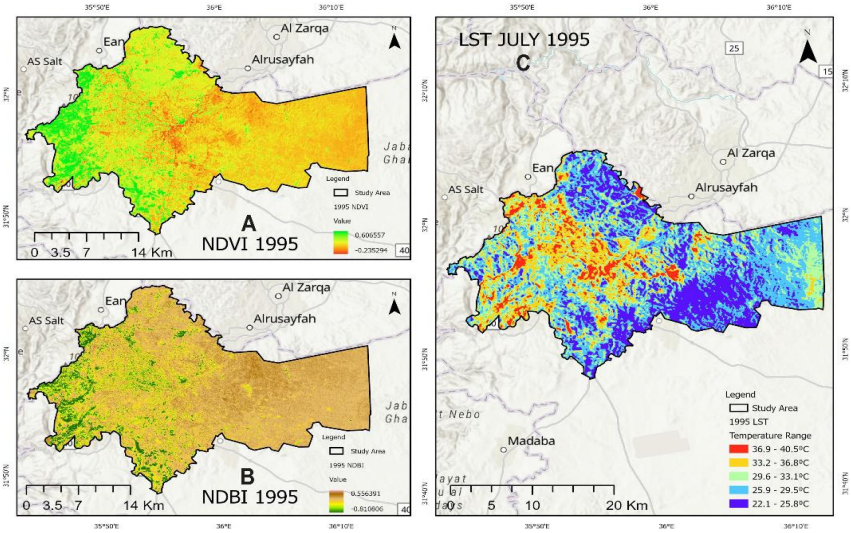

Figure 6. Amman's spatial distribution of NDVI, NDBI and LST in 1995 (Source: Authors primary data Analysis, 2022)

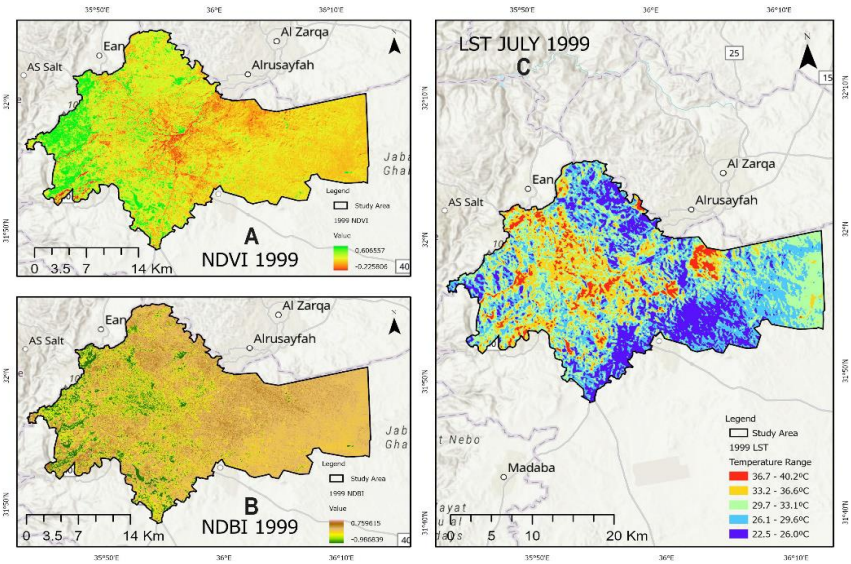

Figure 7. Amman's spatial distribution of NDVI, NDBI, and LST in 1999 (Source: Authors primary data Analysis, 2022)

The results of the LST investigation show that urbanization increases LST by replacing natural vegetation with non-evaporating, non-transpiring surfaces like soil, concrete, and cemented buildings, among others. Due to the dryness of these non-evapotranspiration materials in the urban environment, there is fluctuation in LST within the research region.

4. Spatio-temporal distribution of LST in Amman city

Tables from 3- 9 shows the spatio-temporal areal coverage of the different LST range in Amman city from 1990 to 2022, the statistical data was extracted from the LST analysis.

Table 3. Spatio-temporal distribution of LST in Amman city in 1990

Temperature Range	Area (Km^2)
23.8 - 25.2ºC	34.08
25.3 - 29.5ºC	586.20
29.6 -33.8ºC	2.71
33.9 - 37.2ºC	168.07
37.3 - 39.5ºC	4.91

Table 4. Spatio-temporal distribution of LST in Amman city in 1995

Temperature Range	Area (Km^2)
22.1 - 25.8ºC	2.28
25.9 - 29.5ºC	69.79
29.6 - 33.1ºC	250.92
33.2 - 36.8ºC	414.00
36.9 - 40.5ºC	58.98

Table 5. Spatio-temporal distribution of LST in Amman city in 1999

Temperature Range	Area (Km^2)
22.5 - 26ºC	69.61
26.1 - 29.6ºC	462.35
29.7 - 33.1ºC	240.36
33.2 - 36.6ºC	22.43
36.7 - 40.2ºC	1.22

Table 6. Spatio-temporal distribution of LST in Amman city in 2004

Temperature Range	Area (Km^2)
26 - 29.9ºC	46.38
30 - 33.9ºC	1.88
34 - 37.9ºC	272.24
38 - 41.9ºC	424.59
42 - 45.8ºC	50.88

Table 7. Spatio-temporal distribution of LST in Amman city in 2013

Temperature Range	Area (Km^2)
26.2 - 30.4ºC	61.55
30.5 - 34.6ºC	1.04
34.7 - 38.8ºC	449.25
38.9 - 43.0ºC	29.44
43.1 - 47.3ºC	254.69

(Source: Authors primary data analysis, 2022 Data source: Extracted from the 2022 LST analysis)

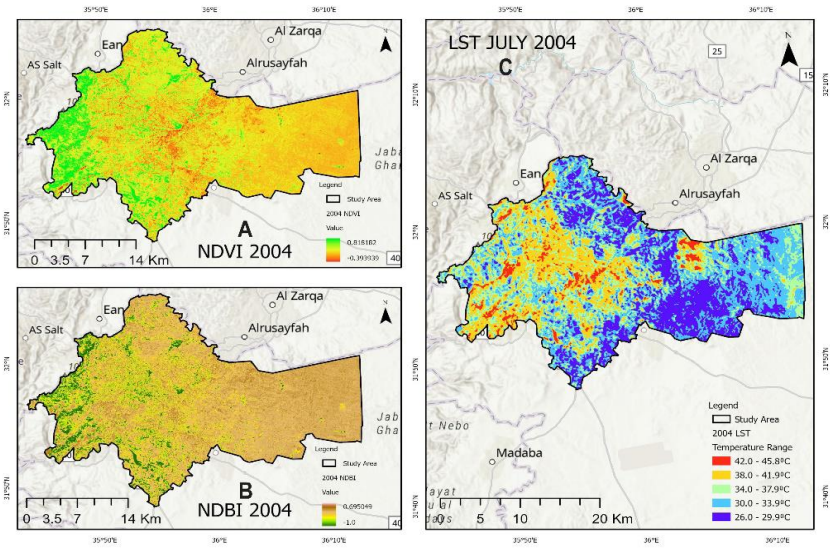

Figure 8. Amman's Spatial distribution of NDVI, NDBI and LST in 2004(Source: Authors primary data Analysis, 2022)

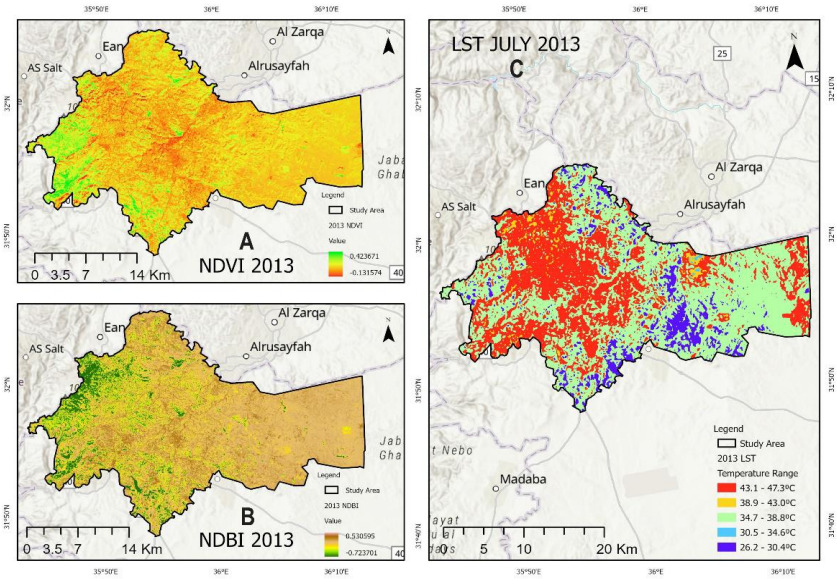

Figure 9. Amman spatial distribution of NDVI, NDBI and LST in 2013 (Source: Authors primary data Analysis, 2022)

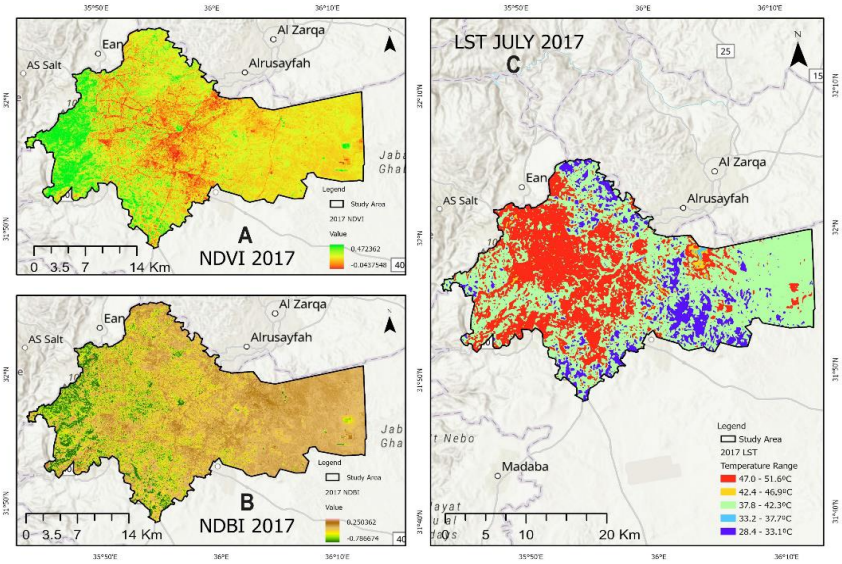

Figure 10: Amman's spatial distribution of NDVI, NDBI and LST in 2017 (Source: Authors primary data Analysis, 2022)

Table 8. Spatio-temporal distribution of LST in Amman city in 2017

Temperature Range	Area (Km^2)
28.4 - 33.1ºC	74.83
33.2 - 37.7ºC	19.88
37.8 - 42.3ºC	462.50
42.4 - 46.9ºC	5.99
47 - 51.6ºC	232.77

Table 9. Spatio-temporal distribution of LST in Amman city in 2022

Temperature Range	Area (Km^2)
26.3 - 30.2ºC	30.10
30.3 - 34.1ºC	2.49
34.2 - 38.1ºC	400.25
38.2 - 42.0ºC	26.43
42.1 - 46.0ºC	336.70

Source: Authors primary data analysis, 2022; Data source: Extracted from the 2022 LST analysis

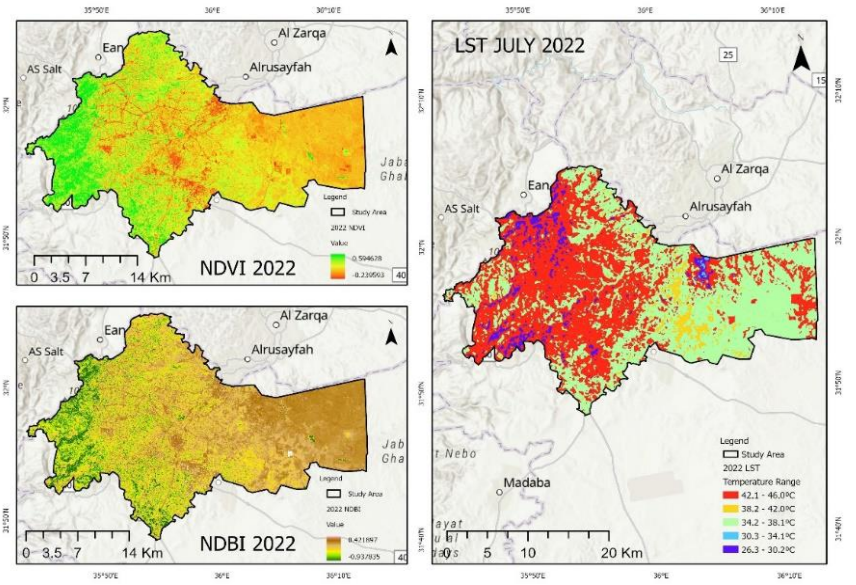

Figure 11. Amman spatial distribution of NDVI, NDBI and LST in 2022 (Source: Authors analysis, 2022)

5. Relationship between NDBI, LST and NDVI in Amman city

To determine the connection between LST, NDVI and NDBI, Pearson's correlation has been applied. The Pearson correlation coefficient quantifies the linear relationship between two data recordings, X and Y. It has a value between -1 and +1, where 1 shows a strong positive correlation, which indicates a strong negative correlation. A correlation coefficient between LST and NDVI, LST and NDBI has been calculated to examine the effects of the land built and agricultural on the temperature of the land surface. Table 10 shows the results of the statistical analysis carried out. Table 10 compares Pearson's correlation coefficients to Spearman's rank correlation coefficients for the LST-NDVI and LST-NDBI relationships.

Table 10. Pearson and Spearman correlation between LST with NDVI and LST with NDBI

Year	LST-NDVI		LST-NDBI	
	Pearson's r	**Spearman's r**	**Pearson's r**	**Spearman's r**
1990	-0.99	-1.00	0.9931	1.00
1995	-1.00	-1.00	1.00	1.00
1999	-1.00	-1.00	1.00	1.00
2004	-1.00	-1.00	1.00	1.00
2013	-1.00	-1.00	1.00	1.00
2017	-1.00	-1.00	1.00	1.00
2022	-1.00	-1.00	1.00	1.00

The result of the correlation coefficient, as shown in Table 10, shows that between 1990 and 2022, there is a significant correlation between NDBI (built) and LST (earth temperature). The fact that LST and NDBI are positively correlated suggests that the research area's built-up urban area can enhance the influence of land surface temperature. Given that a consistent increase in urban area between the study years corresponds to an equivalent increase in land surface temperature, this result explains how urban sprawl and growth affect the environment. The correlation coefficient result, on the other hand, shows that there is a significant negative relationship between the NDVI (agriculture land) and LST (land temperature) between 1990 and 2022. The inverted correlation between NDVI and LST implies that green areas can reduce the impact on the land surface temperature as an increase in agriculture and vegetation covers leads to a decrease in surface temperature and vice versa. The relationship between NDBI, LST, and NDVI shows that increasing the NDBI value increases the LST value and vice versa. Furthermore, Increasing the NDVI value causes the LST value to decrease, and vice versa.

6. Spatial distribution of road network in Amman city (1990 - 2022)

As shown in table 11 below, in year 1990 Amman city has a total road length of 173.42 km, 220.95 3km and 246.20 km in year 1995 and 1999 respectively, in year 2004 the total road length increased to 305.95 km. In year 2013 it became 453.91 km, wheras in 2017 and 2022 Amman city recorded the same total length of road network of 556.51 km. This result shows that within the study year (1990 - 2022) because of the increase in population and road demand, there has been an increase in the construction of road networks. Figure 12 depicts the spatial distribution of Amman's road network during the study years.

Table 11. Length of road network in Amman city per study years (Source: Authors analysis, 2022)

Year	Length of Road
1990	173.42 km
1995	220.95 km
1999	246.20 km
2004	305.95 km
2013	453.91 km
2017	556.51 km
2022	556.51 km

7. Spatial relationship between road network and built-up area in Amman (1990 - 2022)

As shown in figure 13 below, the development of the road networks and built-up area has a direct relationship i.e there is a corresponding increase in built up area and road network. The result shows that in year 1990 Amman city has a total road length of 173.42km with a built-up extent of 107.32km^2. In 1995, there was a total road length of 220.95km and a built-up area of 139.25km^2, in 1999 there was a total road length of 246.2km and a built-up area of 152.54km^2. In 2004 there was a total road length of 305.95km and a built-up area of 178.18km^2. Furthermore, in 2013 there was a total road length of 453.91km and a built-up area of 204.03km^2. On the other hand, there was an equal total road length of 556.51km in 2017 and 2022, with a built-up area of 233.90km^2 and 257.35km^2 respectively. This result explains that increase in construction of road network attract land development and further result to the spread of unplanned settlement (sprawl). Figure 14 shows the spatial distribution of the network of roads and built-up area in Amman city during the study year.

8. Correlation between the road network and the built-up area in Amman city (1990 - 2022)

Pearson's correlation method was employed to generate the correlation between road network and built-up area. The results of the correlation analysis are shown in Table 12.

Table 12. The overall result of the correlation between the road network and built-up area (Source: Authors Analysis, 2022)

Year	Road/Built-up
1990 - 2022	0.98

Table 12 shows a robust positive correlation (0.98) between the extent of the network of roads and the built-up area in Amman during the study year (1990 - 2022). This finding explains how land development has spread as a result of increased road construction.

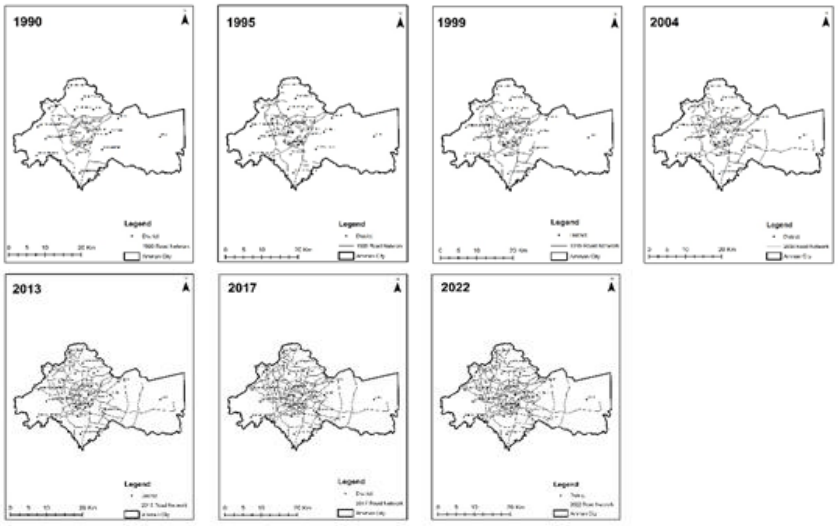

Figure 12. Spatial distribution of road network in Amman city between 1990 and 2022 (Source: Authors analysis, 2022 Based on the road data digitized from aerial photographs)

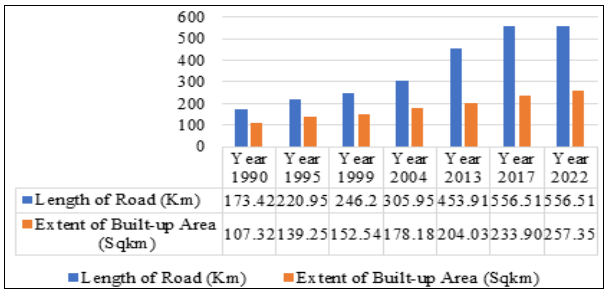

Figure 13. Relationship between the road network and the built-up area in Amman city between 1990 and 2022 (Source: Authors analysis, 2022; Based on the road data digitized from aerial photographs)

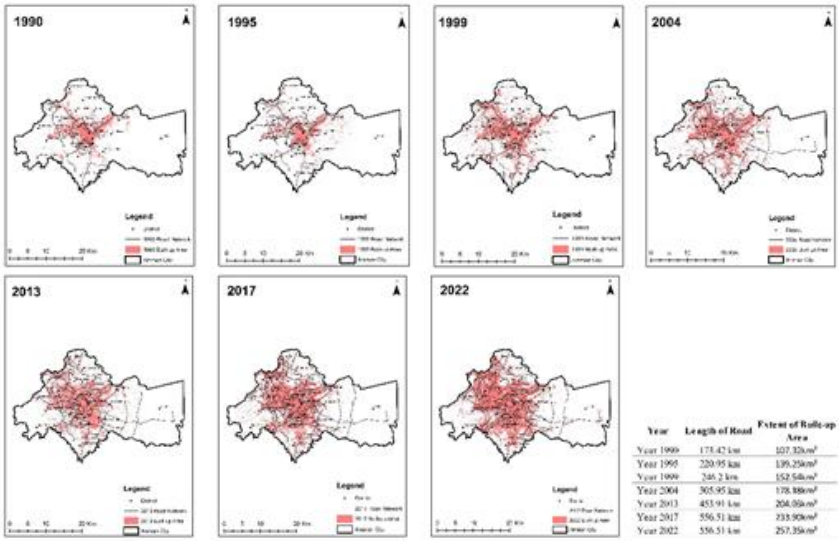

Figure 14. Spatial distribution of the road network and the built-up area in Amman city (1990 - 2022) (Source: Authors analysis, 2022; Data source: Aerial photographs and Landsat Imagery)

CONCLUSIONS AND RECOMMENDATIONS

Given the complexity of the urban surface (buildings, roof tops, farms, etc.), GIS and RS techniques are crucial for studying urban climate. Due to the challenge of obtaining a representative measure of surface temperature, air temperature data from meteorological stations are typically located at the airport, which is frequently cited at the edge of cities. Due to the heterogeneous nature of the urban surface, it is additionally challenging and time-consuming to obtain climatic data for urban areas. Because of this, the analysis of surface temperature using GIS and RS is crucial for identifying how urban sprawl affects the environment. This research also demonstrates how GIS and RS can be used to estimate how the road network will affect urban sprawl and the environment.

Parameters such as NDVI and NDBI, which extract information on greenness and imperviousness, can be used to demonstrate the spatiotemporal changes in land-cover patterns and, when combined with LST data, show the environmental effects of urban sprawl. Effort was made to determine the NDBI, LST, and NDVI for Amman.The study demonstrates that a decline in agricultural land is caused by a proportionate increase in built-up area. The findings of the NDVI analysis explains that there has been variation in vegetation index during the study year due to human activities and also climatic change. Result from this study shows that a proportional growth in built-up area result to a reduction in agriculture land. The estimated NDVI and NDBI maps indicated that Amman city steadily witnessed rapid urbanization and urban sprawl as built-up areas increased from 1990 to 2022, vegetation reduced.

The estimated LST maps revealed that surface temperatures in Amman city have been on the increase from 1990 to 2022 (25.2ºC– 46.0ºC). The high LST dominates the surface of the city, especially within the built-up areas, and the lower LST dominates areas with green cover (vegetation and agricultural land). Therefore, changes in LST is an essential indicator that can be utilized for assessment environmental quality as well as development of socio-economic policy.

Amman's rising surface temperature is a result of the conversion of agricultural and bare land into developed regions to meet the needs of the city's expanding population. However, since the LST is one of the crucial variables for the investigation of urban morphology, the findings of this study clearly demonstrate that the LST varies in distance and time. Given the strong positive link between NDBI and LST, it follows that land surface temperature will rise as urbanization increases. In order to mitigate the effects of LST, towns should create more green spaces in densely populated metropolitan areas.

Our new results show that the built-up area (as an indicator of urbanization) and the vegetated area play a crucial role in assessing the effects of urbanization and human activity on the environment by estimating the temperature of surface. Another finding is that as built-up land increase within the city center, temperature also increases. This factor can be measured only by correlating the NDBI and NDVI factor with LST. Our finding proof that urbanization shows a key part in the occurrence of urban sprawl as this work demonstrates that there is a strong positive correlation between road network and built-area (0.98). Built-up areas increase proportionately to the extent of road network (accessibility) through urbanization process which has adverse socio-economic and environmental impact. Since urbanization cannot be stopped, but it can be sustainably redirected with the proper urban planning, management, and application of policies, and this study is an attempt in that direction. To stop the current condition of land cover change, immediate action must be done by creating a sustainable city plan. Greater Amman municipality should set the goal of becoming a sustainable model city and take appropriate measures to achieve it. Some of the recommendations include the following:

a. The necessity for local governments to encourage afforestation initiatives to increase the amount of green space that reduce the impact of high LST.

b. Since 14% of Greater Amman still falls under the category of agricultural land. For sustainable development, planners and decision-makers should place a high priority on reducing urban sprawl and preserving the remaining agricultural lands and supporting policies related to the development of urban agriculture and incentives to the public and private sectors.

c. Support smart growth initiatives: Smart growth initiatives focus on compact development and redevelopment of built-up areas in cities.

d. incorporating green and cool roofing techniques into building designs because of their high albedos and low heat absorption.

e. Urban managers and planners should start redesigning cities so that many parks, buffer zones, gardens, orchards, and open spaces will be included in the city's physical plans.

f. Finally, it is recommended that Amman municipality adopt effective data management experiences, regulations, and policies from developed countries as well as successful developing countries in which Amman shares the same city feature to reduce the adverse environmental impacts of urbanization and enhance the sustainability of Amman city.

Limitations

Since LST and NDVI can be affected by a wide variety of environmental factors, future research should characterize these factors The results of this study are only applicable to cities with similar characteristics to Amman, which is another limitation. Therefore, to verify these findings, additional research that considers cities with various morphological features should be carried out.

REFERENCES

Abdeljawad, N., Adedokun, V., & Nagy, I. (2022). Managing, assessing and monitoring urban sprawl using remote sensing; change detection, urban expansion intensity index (ueii), and shannon entropy: a case study of Amman city, Jordan (1990–2022). *Journal of Southwest Jiaotong University*, 57(6). https://www.jsju.org/index.php/journal/article/view/1417

Abdullah, S., Barua, D., Abdullah, Sk. Md. A., & Rabby, Y.W. (2022). Investigating the Impact of Land Use/Land Cover Change on Present and Future Land Surface Temperature (LST) of Chittagong, Bangladesh. *Earth Systems and Environment*, 6(1), 221–235. https://doi.org/10.1007/s41748-021-00291-w

Abebe, S., Minale, A.S., & Teketay, D. (2021). Spatio-temporal bamboo forest dynamics in the Lower Beles River Basin, north-western Ethiopia. *Remote Sensing Applications: Society and Environment*, 23, 100538. https://doi.org/10.1016/j.rsase.2021.100538

Aboelata, A., & Sodoudi, S. (2020). Evaluating the effect of trees on UHI mitigation and reduction of energy usage in different built up areas in Cairo. *Building and Environment*, 168, 106490. https://doi.org/10.1016/j.buildenv.2019.106490

Al-Bilbisi, H. (2019). Spatial Monitoring of Urban Expansion Using Satellite Remote Sensing Images: A Case Study of Amman City, Jordan. *Sustainability*, 11(8):2260. https://doi.org/10.3390/su11082260

Al-Kofahi, S.D., Hammouri, N., Sawalhah, M.N., Al-Hammouri, A.A., & Aukour, F.J. (2018a). Assessment of the urban sprawl on agriculture lands of two major municipalities in Jordan using supervised classification techniques. *Arabian Journal of Geosciences*, 11(3), 45. https://doi.org/10.1007/s12517-018-3398-5

Al-Kofahi, S.D., Jamhawi, M.M., & Hajahjah, Z.A. (2018b). Investigating the current status of geospatial data and urban growth indicators in Jordan and Irbid municipality: Implications for urban and environmental planning. *Environment, Development and Sustainability*, 20(3), 1067–1083. https://doi.org/10.1007/s10668-017-9923-y

Chakraborty, T., Lee, X., Ermida, S., & Zhan, W. (2021). On the land emissivity assumption and Landsat-derived surface urban heat islands: A global analysis. *Remote Sensing of Environment*, 265, 112682. https://doi.org/10.1016/j.rse.2021.112682

Chrysoulakis, N., Feigenwinter, C., Triantakonstantis, D., Penyevskiy, I., Tal, A., Parlow, E., Fleishman, G., Düzgün, S., Esch, T., & Marconcini, M. (2014). A Conceptual List of Indicators for Urban Planning and Management Based on Earth Observation. ISPRS *International Journal of Geo-Information*, 3(3), Article 3. https://doi.org/10.3390/ijgi3030980

Correia Filho, W.L.F., Santiago, D., de B., Oliveira-Júnior, J.F. de, Silva Junior, C.A. da, Oliveira, S.R. da S., Silva, E.B. da, & Teodoro, P.E. (2021). *Analysis of environmental degradation in Maceió-Alagoas, Brazil via orbital sensors: A proposal for landscape intervention based on urban afforestation.* Remote Sensing Applications: Society and Environment, 24, 100621. https://doi.org/10.1016/j.rsase.2021.100621

Cox, D.T.C., Shanahan, D.F., Hudson, H.L., Fuller, R.A., & Gaston, K.J. (2018). The impact of urbanisation on nature dose and the implications for human health. *Landscape and Urban Planning*, 179, 72–80. https://doi.org/10.1016/j.landurbplan.2018.07.013

Deng, Y., Wang, S., Bai, X., Tian, Y., Wu, L., Xiao, J., Chen, F., & Qian, Q. (2018). *Relationship among land surface temperature and LUCC*, NDVI in typical karst area. Scientific Reports, 8(1), 1–12.

Dobbs, C., Nitschke, C., & Kendal, D. (2017). Assessing the drivers shaping global patterns of urban vegetation landscape structure. *Science of the Total Environment*, 592, 171–177. https://doi.org/10.1016/j.scitotenv.2017.03.058

DOS (Department of Statistics). *Estimated Population of the Kingdom by Governorate, Locality, Sex and Households*, 2021. 2021. http://dosweb.dos.gov.jo/DataBank/Population_Estimares/PopulationEstimatesbyLocality.pdf (accessed: 31 December 2022).

El Garouani, A., Mulla, D.J., El Garouani, S., & Knight, J. (2017). *Analysis of urban growth and sprawl from remote sensing data: Case of Fez, Morocco.* International Journal of Sustainable Built Environment, 6(1), 160–169.

Escobedo, F.J., Palmas-Perez, S., Dobbs, C., Gezan, S., & Hernandez, J. (2016). Spatio-Temporal Changes in Structure for a Mediterranean Urban Forest: Santiago, Chile 2002 to 2014. *Forests*, 7(6), 121. https://doi.org/10.3390/f7060121

Estoque, R.C., Murayama, Y., & Myint, S.W. (2017). Effects of landscape composition and pattern on land surface temperature: An urban heat island study in the megacities of Southeast Asia. *Science of the Total Environment*, 577, 349–359. https://doi.org/10.1016/j.scitotenv.2016.10.195

Gazi, Md. Y., Rahman, Md. Z., Uddin, Md. M., & Rahman, F.M.A. (2021). Spatio-temporal dynamic land cover changes and their impacts on the urban thermal environment in the Chittagong metropolitan area, Bangladesh. *GeoJournal*, 86(5), 2119–2134. https://doi.org/10.1007/s10708-020-10178-4

Gui, X., Wang, L., Yao, R., Yu, D., & Li, C. (2019). Investigating the urbanization process and its impact on vegetation change and urban heat island in Wuhan, China. *Environmental Science and Pollution Research*, 26(30), 30808–30825. https://doi.org/10.1007/s11356-019-06273-w

Hameed, S.A., Ahmed, S.R., & Liaqut, A. (2019). Analytical Review of Land Use Changes by Remote Sensing and GIS Techniques in District Gujrat, Pakistan. *Int. J. Econ. Environ. Geol.*, 10(2), 118–123.

Han, X., Huang, X., Liang, H., Ma, S., & Gong, J. (2018). Analysis of the relationships between environmental noise and urban morphology. *Environmental Pollution*, 233, 755–763. https://doi.org/10.1016/j.envpol.2017.10.126

Imran, H.M., Hossain, A., Islam, A.K.M.S., Rahman, A., Bhuiyan, M.A.E., Paul, S., & Alam, A. (2021). Impact of Land Cover Changes on Land Surface Temperature and Human Thermal Comfort in Dhaka City of Bangladesh. *Earth Systems and Environment*, 5(3), 667–693. https://doi.org/10.1007/s41748-021-00243-4

Jaber, S.M. (2018). Landsat-based vegetation abundance and surface temperature for surface urban heat island studies: The tale of Greater Amman Municipality. *Annals of GIS*, 24(3), 195–208. https://doi.org/10.1080/19475683.2018.1471519

Jaber, S.M. (2020). Is there a relationship between human population distribution and land surface temperature? Global perspective in areas with different climatic classifications. *Remote Sensing Applications: Society and Environment*, 20, 100435. https://doi.org/10.1016/j.rsase.2020.100435

Janhäll, S. (2015). Review on urban vegetation and particle air pollution – Deposition and dispersion. *Atmospheric Environment*, 105, 130–137. https://doi.org/10.1016/j.atmosenv.2015.01.052

Jiménez-Muñoz, J.C., Sobrino, J.A., Skoković, D., Mattar, C., & Cristóbal, J. (2014). Land Surface Temperature Retrieval Methods From Landsat-8 Thermal Infrared Sensor Data. *IEEE Geoscience and Remote Sensing Letters*, 11(10), 1840–1843. https://doi.org/10.1109/LGRS.2014.2312032

Khawaldah, H.A. (2016). A Prediction of Future Land Use/Land Cover in Amman Area Using GIS-Based Markov Model and Remote Sensing. *Journal of Geographic Information System, 8*(3), Article 3. https://doi.org/10.4236/jgis.2016.83035

Kaplan, G., Avdan, U., & Avdan, Z.Y. (2018). *Urban Heat Island Analysis Using the Landsat 8 Satellite Data: A Case Study in Skopje, Macedonia*. Proceedings, 2(7), Article 7. https://doi.org/10.3390/ecrs-2-05171

Kumari, B., Tayyab, M., Shahfahad, Salman, Mallick, J., Khan, M.F., & Rahman, A. (2018). Satellite-Driven Land Surface Temperature (LST) Using Landsat 5, 7 (TM/ETM+ SLC) and Landsat 8 (OLI/TIRS) Data and Its Association with Built-Up and Green Cover Over Urban Delhi, India. *Remote Sensing in Earth Systems Sciences*, 1(3), 63–78. https://doi.org/10.1007/s41976-018-0004-2

Kundu, K., Halder, P., & Mandal, J.K. (2021). Change Detection and Patch Analysis of Sundarban Forest During 1975–2018 Using Remote Sensing and GIS Data. *SN Computer Science*, 2(5), 364. https://doi.org/10.1007/s42979-021-00749-8

Momin, H., Tamang, C., Biswas, R., & Odud, A. (2022). Analyzing Land-Use/Land-Cover Changes and Its Impact on Land Surface Temperature in Berhampore Municipality, West Bengal, India. *Sustainable Urbanism in Developing Countries*, CRC Press.

Mushore, T.D., Odindi, J., Dube, T., Matongera, T.N., & Mutanga, O. (2017). Remote sensing applications in monitoring urban growth impacts on in-and-out door thermal conditions: A review. *Remote Sensing Applications: Society and Environment*, 8, 83–93. https://doi.org/10.1016/j.rsase.2017.08.001

Nse, O.U., Okolie, C.J., & Nse, V.O. (2020). Dynamics of land cover, land surface temperature and NDVI in Uyo City, Nigeria. *Scientific African*, 10, e00599. https://doi.org/10.1016/j.sciaf.2020.e00599

Patarkalashvili, T.K. (2017). Urban forests and green spaces of Tbilisi and ecological problems of the city. *Annals of Agrarian Science*, 15(2), 187–191. https://doi.org/10.1016/j.aasci.2017.03.003

Potter, R.B., Darmame, K., Barham, N., & Nortcliff, S. (2009). "Ever-growing Amman", Jordan: Urban expansion, social polarisation and contemporary urban planning issues. *Habitat International*, 33(1), 81–92. https://doi.org/10.1016/j.habitatint.2008.05.005

Richards, D.R., & Belcher, R.N. (2020). Global Changes in Urban Vegetation Cover. *Remote Sensing*, 12(1). https://doi.org/10.3390/rs12010023

Rouse, J.W., Haas, R.H. Schell, J.A. & Deering, D.W. (1974). *Monitoring Vegetation Systems in the Great Plains with ERTS.* Third Earth Resources Technology Satellite-1 Symposium, Volume I: Technical Presentations, Section A, NASA SP-351, 309–317. https://ntrs.nasa.gov/citations/19740022614

Semeraro, T., Scarano, A., Buccolieri, R., Santino, A., & Aarrevaara, E. (2021). *Planning of Urban Green Spaces.* An Ecological Perspective on Human Benefits. Land, 10(2), Article 2. https://doi.org/10.3390/land10020105

Ullah, M., Li, J., & Wadood, B. (2020). Analysis of Urban Expansion and its Impacts on Land Surface Temperature and Vegetation Using RS and GIS, A Case Study in Xi'an City, China. *Earth Systems and Environment*, 4(3), 583–597. https://doi.org/10.1007/s41748-020-00166-6

USGS. (2019a). *Landsat 8 (L8) Data Users Handbook Version 5.0. EROS Sioux Falls*. South 17.

USGS. (2019b). *Landsat 7 (L7) Data Users Handbook Version 2.0. EROS Sioux Falls.* South Dakota, USA, 114.

Vani, M., & Prasad, P.R.C. (2020). Assessment of spatio-temporal changes in land use and land cover, urban sprawl, and land surface temperature in and around Vijayawada city, India. *Environment, Development and Sustainability*, 22(4), 3079–3095. https://doi.org/10.1007/s10668-019-00335-2

Wang, V.S., Lo, E.W., Liang, C.H., Chao, K.P., Bao, B.Y., & Chang, T.Y. (2016). Temporal and spatial variations in road traffic noise for different frequency components in metropolitan Taichung, Taiwan. *Environmental Pollution*, 219, 174–181. https://doi.org/10.1016/j.envpol.2016.10.055

Xu, R., Hu, Y., Gao, H., & Pan, Z. (2017). Derivation of fractional urban signals in better capturing urbanization process. *Environmental Earth Sciences*, 76(12), 412. https://doi.org/10.1007/s12665-017-6747-x

Yan, Z.W., Wang, J., Xia, J.J., & Feng, J.M. (2016). Review of recent studies of the climatic effects of urbanization in China. *Advances in Climate Change Research*, 7(3), 154–168. https://doi.org/10.1016/j.accre.2016.09.003

Zhan, X., & Ukkusuri, S.V. (2019). Spatial Dependency of Urban Sprawl and the Underlying Road Network Structure. *Journal of Urban Planning and Development*, 145(4), 04019014. https://doi.org/10.1061/(ASCE)UP.1943-5444.0000526

Article history: Received: 12.11.2022 Revised: 09.01.2023 Accepted: 09.03.2023 Available online: 22.03.2023